

Article

Mechanism and Performance of the SCR of NO with NH₃ over Sulfated Sintered Ore Catalyst

Wangsheng Chen ^{1,2}, Fali Hu ^{1,2}, Linbo Qin ^{1,2}, Jun Han ^{1,2,*} , Bo Zhao ^{1,2}, Yangzhe Tu ^{1,2} and Fei Yu ³ 

¹ School of Resource and Environmental Engineering, Wuhan University of Science and Technology, Wuhan 430081, China; chenwangsheng@wust.edu.cn (W.C.); hufali@hotmail.com (F.H.); qinlinbo@wust.edu.cn (L.Q.); zhaobo87@wust.edu.cn (B.Z.); tuyangzhe123@hotmail.com (Y.T.)

² Industrial Safety Engineering Technology Research Center of Hubei Province, Wuhan University of Science and Technology, Wuhan 430081, China

³ Department of Agricultural and Biological Engineering, Mississippi State University, Mississippi State, MS 39762, USA; fyu@abe.msstate.edu

* Correspondence: hanjun@wust.edu.cn; Tel.: +86-27-6886-2880

Received: 25 December 2018; Accepted: 14 January 2019; Published: 16 January 2019



Abstract: A sulfated sintered ore catalyst (SSOC) was prepared to improve the denitration performance of the sintered ore catalyst (SOC). The catalysts were characterized by X-ray Fluorescence Spectrometry (XRF), Brunauer–Emmett–Teller (BET) analyzer, X-ray diffraction (XRD), X-ray photoelectron spectroscopy (XPS) and diffuse reflectance infrared spectroscopy (DRIFTS) to understand the NH₃-selective catalytic reduction (SCR) reaction mechanism. Moreover, the denitration performance and stability of SSOC were also investigated. The experimental results indicated that there were more Brønsted acid sites at the surface of SSOC after the treatment by sulfuric acid, which lead to the enhancement of the adsorption capacity of NH₃ and NO. Meanwhile, Lewis acid sites were also observed at the SSOC surface. The reaction between –NH₂, NH₄⁺ and NO (E-R mechanism) and the reaction of the coordinated ammonia with the adsorbed NO₂ (L-H mechanism) were attributed to NO_x reduction. The maximum denitration efficiency over the SSOC, which was about 92%, occurred at 300 °C, with a 1.0 NH₃/NO ratio, and 5000 h^{−1} gas hourly space velocity (GHSV).

Keywords: sintered ore catalyst; sulfate; In-situ DRIFTS; SCR

1. Introduction

Nitrogen oxide (NO_x) is one of the major atmospheric pollutants and is mainly generated from the combustion of fossil fuel, which has serious harmful effects on human health and the ecological environment. In 2016, the total emission of NO_x from the iron and steel industry was about 1.04 million tonnes [1]. The sintering process in iron-making plants uses coal or coke as fuel, which is a major emission source of NO_x. About 35–50% of the total NO_x emission from the iron and steel industry is attributed to the sintering process [2–4]. The new ultra-low emission standard of air pollutants for the iron and steel industry will be issued by Chinese government and require that NO_x concentration in the sintering flue gas should be below 50 mg/m³. Hence, it is urgent to address the treatment of sintering flue gas.

Selective catalytic reduction (SCR) over V₂O₅-WO₃ (MoO₃)/TiO₂ catalyst has been widely applied in power stations because of its high denitration efficiency [5–7]. However, there are still shortcomings such as the toxicity of the catalyst, and the high operation costs [8]. In particular, the reaction temperature of the current commercial catalysts is higher than the temperature of the sintering flue gas [9]. Therefore, the sintering flue gas must be heated to the reaction temperature of the catalyst by using additional fuels.

Many researchers paid more attention to developing the low temperature catalysts or the catalysts prepared by the non-noble metals for sintering flue gas. Zhang et al. reported that the Fe-based catalysts exhibited a high catalytic activity for NO reduction [10]. Wang [11] also stated that the Fe₂O₃ particles had a good performance during NO_x elimination, where the highest NO_x conversion reached 95%. Yang et al. [12] claimed that α-Fe₂O₃ had a poor SCR activity, while γ-Fe₂O₃ had an excellent SCR activity at 200–350 °C. Meanwhile, it was also found that the further increase reaction temperature from 350 to 500 °C would suppress NO_x conversion over γ-Fe₂O₃ [13].

It was well known that the sintered ore was one of the raw materials in the sintering plant, its main component was Fe₂O₃. In our previous study, Han et al. and Chen et al. [14,15] proposed that the hot sintered ore was used as catalysts for NO_x removal from the sintering flue gas. The experimental results illustrated that the hot sintered ore had a good denitration performance, the denitration efficiency was about 60% at 300 °C, with a 1.0 NH₃/NO ratio, and 1000 h⁻¹ GHSV. However, the denitration efficiency was too low and the NO_x concentration from the sintering flue gas could reach the limit after SCR over the sintered ore.

Ciambelli [16] found that introduction of SO₄²⁻ into SCR catalysts can promote the surface acidity of the catalysts. Thus, the catalytic activity was promoted. Khodayari [17] and Xu [18] thought that the sulfation of the catalysts would decrease the oxidization ability of Fe³⁺, and separated the active sites of adsorbing -NH₂ and the active sites of oxidizing -NH₂. Therefore, the catalytic oxidization of NH₃ over γ-Fe₂O₃ was suppressed. This process resulted in an obvious promotion of NO_x conversion. Zhang [19] also investigated the sulfation of CeO₂-ZrO₂, and their experiment results demonstrated that the sulfated CeO₂-ZrO₂ provided more surface acidities and acidic sites, and Brønsted acid sites were also increased.

In order to improve the denitration efficiency, SSOC was prepared and the influence of the acidification on SCR performance was investigated. At the same time, the reaction mechanisms of SCR over SSOC were also discussed.

2. Results and Discussion

2.1. Characterizations

The main components of the two catalysts were shown in Table 1. It presented that the main components of both two catalysts were Fe₂O₃ and CaO. After the introduction of sulfuric acid, the proportion of iron oxide in the catalyst was decreased and sulphate content was significantly increased.

Table 1. Chemical compositions of catalysts (%).

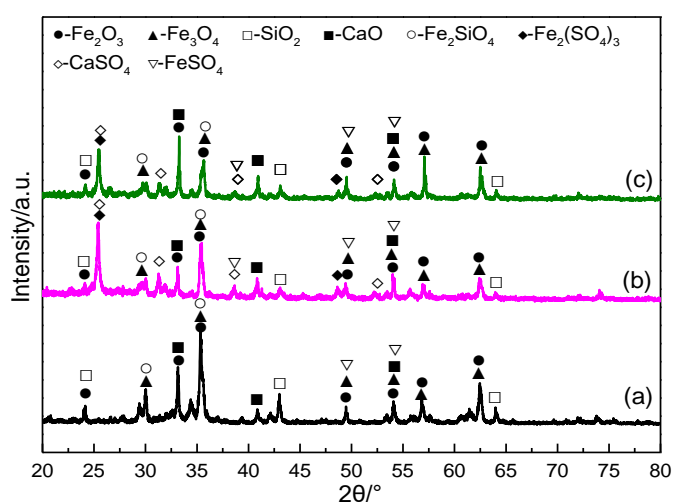
	Fe ₂ O ₃	CaO	SiO ₂	Al ₂ O ₃	MgO	MnO ₂	TiO ₂	P ₂ O ₅	SO _x
SOC	75.42	12.54	4.22	1.19	1.02	0.19	0.20	0.09	0.14
SSOC	48.92	11.52	2.82	0.79	0.85	0.13	0.09	0.05	29.92

The BET surface area, pore-size and pore volume of the catalysts were presented in Table 2. The specific surface area of the SOC was 3.684 m²/g, the total pore volume was 0.00714 cm³/g, and the average pore diameter was 6.3 nm. The BET surface area, pore size and pore volume of the SSOC were 4.734 m²/g, 5.9 nm and 0.00964 cm³/g, respectively. It was indicated that the introduction of sulfuric acid would open some micro-pores, which lead to the increase of the total pore volume. At the same time, the sulphate would block some pores. The BET of SSOC was higher than that of SOC, which meant that the sulfation had a positive effect on the pore structure of SOC.

Table 2. Textural properties of the catalysts.

Catalysts	BET Surface Area (m ² ·g ⁻¹)	Total Pore Volume (cm ³ ·g ⁻¹)	Average Pore Diameter (nm)
SOC	3.684	0.00714	6.3
SSOC	4.734	0.00964	5.9

The XRD patterns of the catalysts were demonstrated in Figure 1. Several sharp diffraction peaks at 24.1°, 33.2°, 35.6°, 49.6°, 54.2°, 57.1° and 62.6° were observed, which were assigned to α -Fe₂O₃ (JCPDS NO. 33-0664), and the characteristic peaks of α -Fe₃O₄ at 30.1°, 33.2°, 49.6°, 54.2° and 57.1° were also detected in Figure 1. The results indicated that the main components of SOC were α -Fe₂O₃ and a small amount of α -Fe₃O₄. After the acidification with sulfuric acid, it could be seen that the peak of α -Fe₂O₃ was decreased. Meanwhile, the characteristic peaks (25.4°, 31.4°, 38.7°, 52.2°) of Fe₂(SO₄)₃ were detected, and a small amount of FeSO₄ and CaSO₄ also appeared.

**Figure 1.** XRD patterns of the catalysts: SOC (a), SSOC (b) and SSOC after tested (c).

X-ray photoelectron spectroscopy (XPS) was used to study the valence states of the catalysts, as shown in Figure 2. It could be seen from Figure 2 (I) that there were obvious peaks of C (1s), O (1s), and Fe (2p) in both of the two catalysts. Moreover, there were obvious S (2p) peaks after the introduction of sulfuric acid. As shown in Figure 2 (II), the binding energies of Fe 2p 2/3 and Fe 2p 1/2 on SOC were mainly centered at about 710.8 and 724.3 eV, which were indications that the iron species were mainly in the form of Fe³⁺ in the SOC [20]. At the same time, a small number of Fe²⁺ existed, which was also consistent with the XRD results. The binding energies of Fe 2p 2/3 and Fe 2p 1/2 of SSOC were higher than those of SOC. The peak of Fe 2p 2/3 appeared at 711.8 eV and the peak of Fe 2p 1/2 appeared at 724.9 eV. After the acidification with sulfuric acid, both Fe₂(SO₄)₃ and FeSO₄ appeared in the SSOC, which contributed to Fe 2p peaks shifting to the higher position. In addition, in Figure 2 (III), the peak of S 2p appeared at 169.3 eV, indicating that sulfur compounds existed in the form of SO₄²⁻ [21].

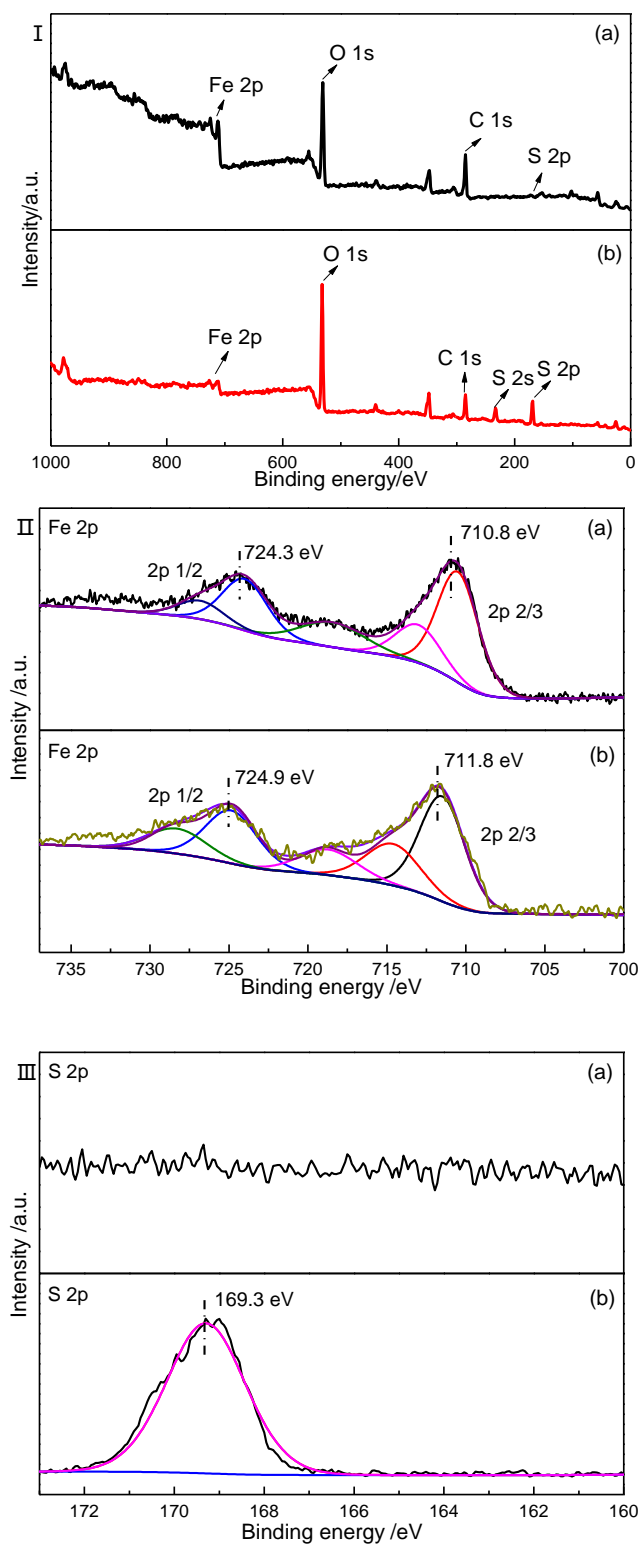


Figure 2. XPS spectra of the catalysts: SOC (a) and SSOC (b).

2.2. In-Situ DRIFTS Studies

2.2.1. Adsorption of NH₃

Figure 3 showed the FTIR spectra of NH₃ adsorption over the SSOC with 1000 ppm NH₃/Ar under different temperatures (250–350 °C). Thirty minutes after NH₃/Ar introduction, the bands at

1690, 1525, 1460 and 1408 cm^{-1} were observed. The bands at 1690, 1460 and 1408 cm^{-1} were symmetric bending vibration of NH_4^+ species at Brønsted acid sites [20,22]. The bands at 1525 and 3434 cm^{-1} were assigned to the intermediate species, such as ammonium or amide species ($-\text{NH}_2$) [20]. Meanwhile, the bands at 3242 and 3120 cm^{-1} could be ascribed to the N–H stretching vibration of coordination NH_3 , and the bands at 1259 cm^{-1} (symmetric bending vibration of NH_3 on Lewis acid sites) and 1102 cm^{-1} (NH_3 species adsorbed on Lewis acid sites) also appeared [20,23,24]. The intensities of the peaks of NH_4^+ species (1690, 1460 and 1408 cm^{-1}) and $-\text{NH}_2$ species (1525 cm^{-1}) first increased and then decreased in the temperature range of 250–350 °C. There were peaks at 960 and 930 cm^{-1} (NH_3 of gaseous state or weak adsorption state) under 300 °C. Yu et al. [25] stated that the following reactions probably took place in the reaction:



According to Equations (1)–(3), the more functional groups formed at the surface of the catalyst, the higher the reaction activity. Thus, the optimum adsorption activity of NH_3 over the SSOC was 300 °C, as shown in Figure 3.

The dependence of FTIR spectra over the SOC and SSOC on the reaction time at 1000 ppm NH_3/Ar and 300 °C was presented in Figure 4. Figure 4a demonstrated that there were 6 bands in the range of 1690–1100 cm^{-1} . The bands at 1690, 1405 and 1454 cm^{-1} were related to the symmetric bending vibration of NH_4^+ species, and the band at 1525 cm^{-1} was ascribed to the intermediate products of ammonium or $-\text{NH}_2$ species. Moreover, the band at 3242 cm^{-1} (N–H stretching vibration of coordinated NH_3) appeared at 10 min. With the feed of NH_3 , the adsorption band at 1259 cm^{-1} (symmetric bending vibration of NH_3 on Lewis acid sites) appeared at 30 min, and the band at 1107 cm^{-1} (NH_3 of gaseous state or weak adsorption state) appeared at 60 min. Hence, there were both Lewis acid sites and Brønsted acid sites on the surface of SOC. The FTIR spectra over SSOC dependence of the reaction time was presented in Figure 4b, and the bands of NH_3 adsorption were basically the same as those of SOC. Moreover, the bands at 3434 cm^{-1} ($-\text{NH}_2$ groups) and 3128 cm^{-1} (coordination NH_3 on Lewis acid sites) were observed because the surface acidity of SSOC was strengthened. There were two new weak bands that appeared at 965 and 927 cm^{-1} , where NH_3 was in a gaseous state or weak adsorption state. These weakly adsorbed or gaseous NH_3 could rapidly adsorbed on the acid sites once the adsorbed NH_3 species was consumed. It could also be seen that the strength of NH_3 adsorption peak was enhanced after SOC acidification with sulfuric acid, which was the reason that the surface acidity of SSOC was enhanced after the acidification. The influence of the acidity of SSOC on the denitration efficiency is presented in Figure 5. The different acidity of SSOC was achieved by sulfating with 1, 3 and 5 mol/L sulfuric acid. In this experimental run, the mass of catalyst and the volume of sulfuric acid were the same. Only the concentration of sulfuric acid was varied. It was demonstrated the maximum denitration efficiency occurred at the catalyst treated by 5 mol/L sulfuric acid, and its denitration efficiency was 92.3% at 300 °C. At the same time, the denitration efficiency of the catalysts sulfated by 1 and 3 mol/L was 56.6% and 68.5% at the same reaction temperature. Moreover, the experimental results proved that the optimum reaction temperature for all catalysts was 300 °C. These sulfates on the surface of SSOC provided more Brønsted acid sites (Peaks at 1690, 1525 cm^{-1} were increased), which promoted the adsorption capacity for NH_3 . Hence, the catalyst denitration performance was also improved [26,27].

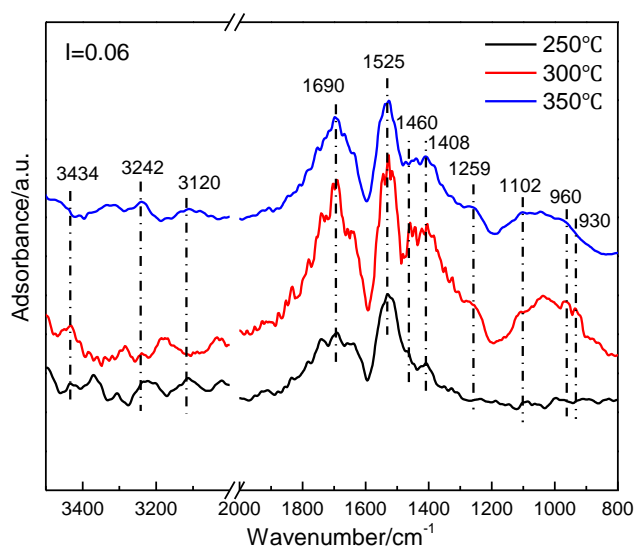


Figure 3. DRIFT spectra of SSOC in the condition of 1000 ppm NH₃ at 250–350 °C for 30 min.

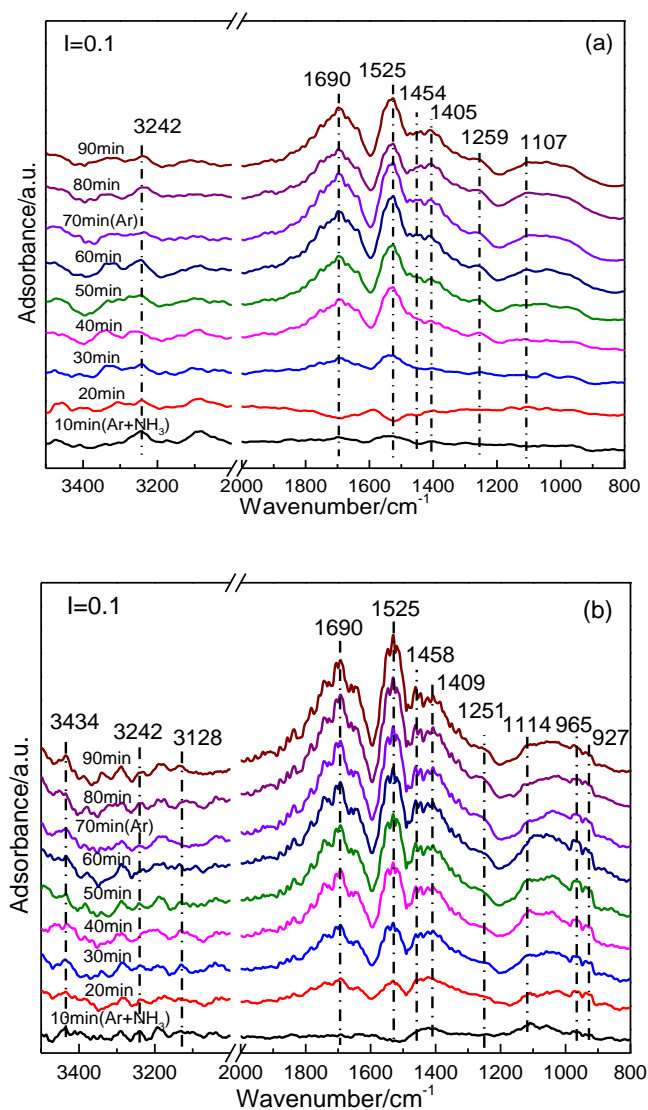


Figure 4. DRIFT spectra of SOC (a) and SSOC (b) exposed to 1000 ppm NH₃ at 300 °C at different time.

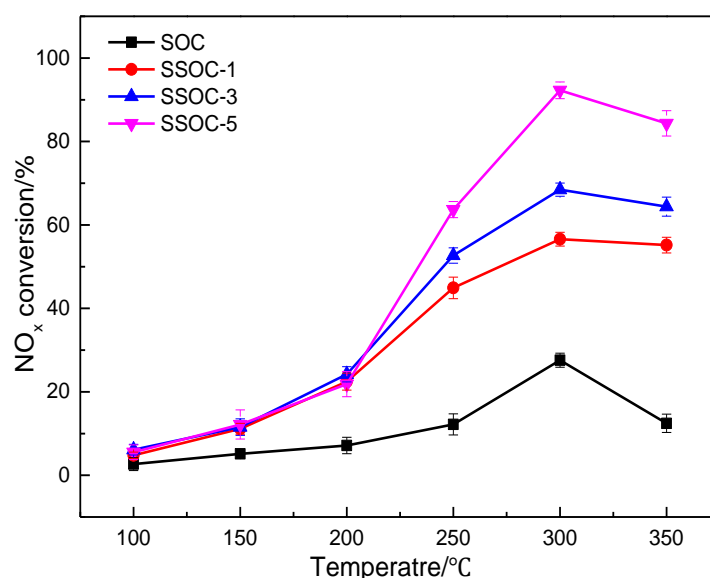
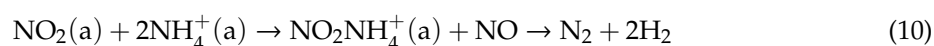
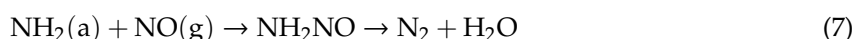
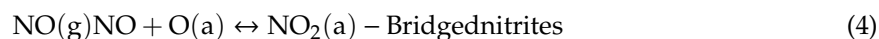


Figure 5. The influence of acidity of SSOC on SCR performance.

2.2.2. Co-Adsorption of NO and O₂

Figure 6 indicated the DRIFTS spectra of co-adsorption of NO and O₂ under 250–350 °C, and 1000 ppm NO + 15% O₂/Ar. After 30 min, there were 4 bands appeared in the range of 1620–1290 cm⁻¹ and a weak band appeared at 1014 cm⁻¹. The band at 1607 cm⁻¹ was ascribed to bridged nitrate species and adsorbed NO₂ molecules [28,29]. The bands at 1485 and 1417 cm⁻¹ were assigned to bidentate nitrates and monodentate nitrates respectively [30–32]. In addition, the bands at 1293 and 1014 cm⁻¹ were related to nitro compounds [31]. The variation trend of the intensities of these bands were same as NH₃ adsorption in the temperature range of 250–350 °C. The adsorption process can be explained by the following formula:



According to Equations (4)–(10), all the peaks in Figure 6 were important to the SCR reaction. The intensity of peaks at 300 °C was the highest, which mean that the optimum adsorption temperature for NO was also 300 °C.

Figure 7 showed the DRIFTS spectra over SOC and SSOC at different reaction times under 300 °C, 1000 ppm NO + 15% O₂/Ar. Similar with the spectra in Figure 6, after 10 min, there were 4 bands that appeared in the range of 1620–1300 cm⁻¹ and a weak band appeared at 1022 cm⁻¹. The bands intensities were gradually increased with the adsorption time. It could be seen that in Figure 7b, the adsorption intensity of SSOC was obviously higher than that of SOC, especially for the nitro compounds (1290 cm⁻¹) and the nitrate species (1490 cm⁻¹). The results indicated that the adsorption capacity of NO was improved after the acidification with sulfuric acid. It had been shown that the introduction of SO₄²⁻ enhanced the adsorption of NO [26].

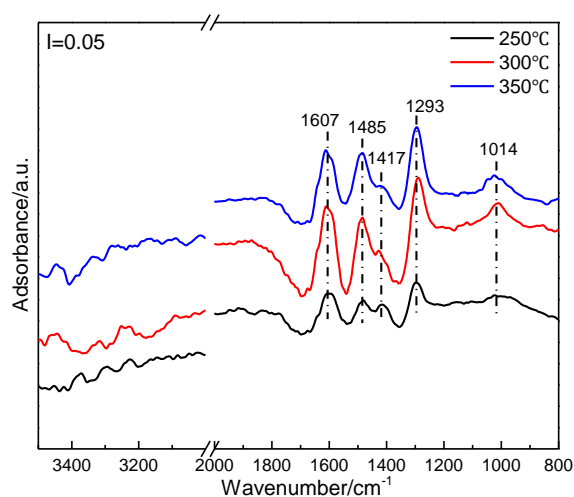


Figure 6. DRIFT spectra of SSOC in the condition of 1000 ppm NO and 15% O₂ at 250–350 °C for 30 min.

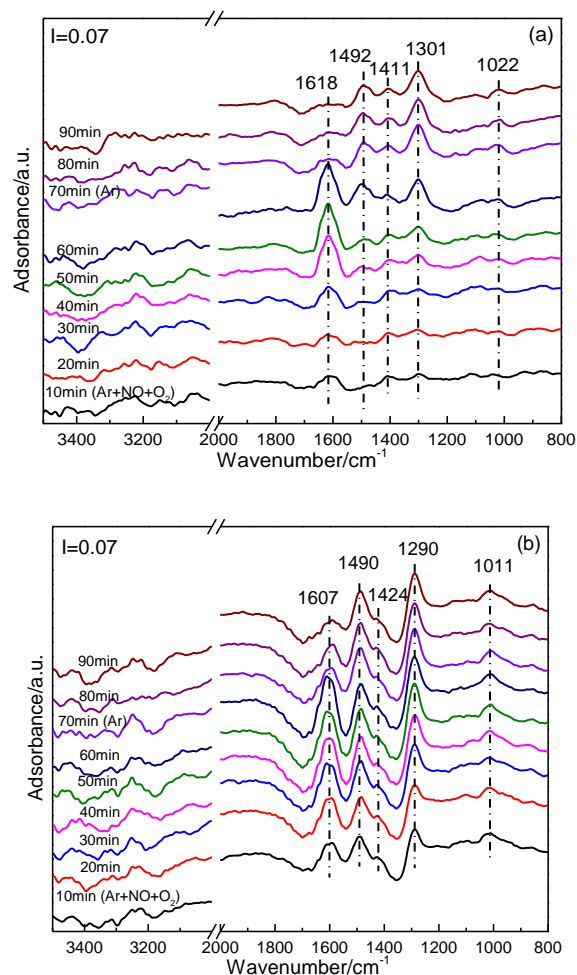


Figure 7. DRIFT spectra of SOC (a) and SSOC (b) exposed to 1000 ppm NO and 15% O₂ at 300 °C for a different time.

The results showed that the peak intensities of the adsorbed species related to NO₂ molecules and bridged nitrate species (1607 and 1618 cm⁻¹) were decreased obviously with purging by Ar, which indicated NO₂ molecules and bridged nitrate species absorbed at the surface of catalysts were unstable.

At the same time, it was found that the intensities of bidentate nitrates, monodentate nitrates and nitro compounds were stable even after an Ar purge.

2.2.3. Reaction between NH_3 and NO

The reaction at the surface of catalyst by introducing NH_3 and $\text{NO} + \text{O}_2$ into an in-situ reactor was also studied. Figure 8 shows that NH_4^+ species (1695 cm^{-1}), amide species ($-\text{NH}_2$) or ammonium (1533 cm^{-1}), and several weak adsorption bands at 1252 , and 3242 cm^{-1} (NH_3 adsorbed on Lewis acid site) were detected on the surface of SOC after NH_3 introduction at 30 min. On the surface of SSOC catalyst, NH_4^+ species at 1695 , 1427 and 1454 cm^{-1} and weakly adsorbed NH_3 or gaseous NH_3 (966 , 925 cm^{-1}) were also detected. There were two bands at 3434 cm^{-1} ($-\text{NH}_2$ groups) and 3127 cm^{-1} (coordination NH_3 on Lewis acid sites) that appeared at the same time. After switching to $\text{NO} + \text{O}_2$, the adsorbed species of NH_3 over SOC and SSOC gradually disappeared and the adsorbed species of NO_x appeared. These bands were ascribed to NO_2 molecules and bridged nitrate species (1602 and 1618 cm^{-1}), bidentate nitrates (1488 and 1498), monodentate nitrates (1413 and 1419 cm^{-1}) and nitro compounds (1290 , 1295 , 1020 and 1011 cm^{-1}). Comparing Figure 8a with Figure 8b, it could be seen that there were more nitrite species and NH_3 species adsorbed at SSOC than those at SOC. This could be explained that the SSOC contained more active sites, which resulted from the sulfates on SSOC, and Equations (7)–(10) occurred [33]. The reaction of amide species ($-\text{NH}_2$) and NH_4^+ species on the surface of catalysts with the gaseous NO was E-R mechanism, and the reaction between adsorbed state NO_2 and adsorbed NH_3 followed L-H mechanism. Therefore, the reaction between NO and NH_3 over SOC and SSOC had two mechanisms.

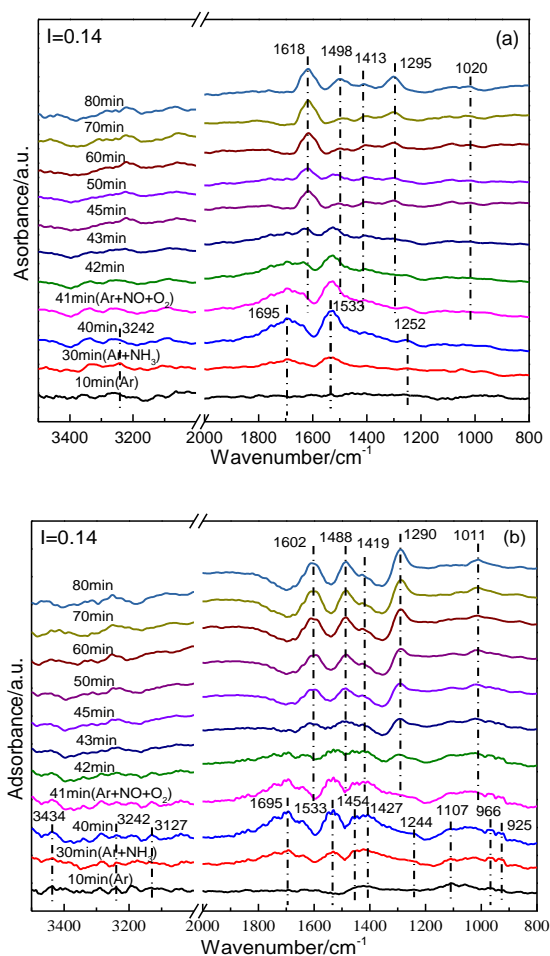


Figure 8. DRIFT spectra of SOC (a) and SSOC (b) successively exposed to 1000 ppm NH_3 , 1000 ppm $\text{NO} + 15\% \text{O}_2$ for different time under $300 \text{ }^\circ\text{C}$.

2.2.4. SCR Performance

SCR performance were carried out in a fixed-bed reactor, which was made of quartz with an inner diameter of 20 mm and a length of 1000 mm. In this experiment, the mass of the catalysts samples was 13.49 g, the flow rate of the flue gas which simulated sintering flue gas was about 600 mL/min, the simulated sintering flue gas contained 300 ppm NO, 15% O₂ and balance N₂. The temperature in the reactor was kept at 100 °C–350 °C, with the condition of a 0.5–1.0 NH₃/NO ratio and 5000 h⁻¹ GHSV. The NO_x concentrations in simulated flue gas at the inlet and outlet of the reactor were continuously recorded by a gas analyzer (PG-350, Horiba, Kyoto, Japan) with an accuracy of ±1.0%. The NO_x conversion was calculated according to the following equations:

$$\text{NO}_x \text{ conversion} = \frac{[\text{NO}_x]_{\text{in}} - [\text{NO}_x]_{\text{out}}}{[\text{NO}_x]_{\text{in}}} \times 100\% \quad (11)$$

Figure 9 presented the denitration performance of SOC and SSOC in the temperature range of 100 °C–350 °C. It was found that the reaction temperature had a great effect on the NH₃-SCR denitration performance of SOC and SSOC. The optimum reaction temperature was 300 °C, which conformed well with the in-situ DRIFTS results. The NO_x conversion of SOC was only 27% at 300 °C, 1.0 NH₃/NO ratio and 5000 h⁻¹ GHSV, and the NO_x conversion of SSOC was 92% at the same condition. It was found that the denitration performance of SSOC was greatly improved and the optimum reaction temperature was 300 °C.

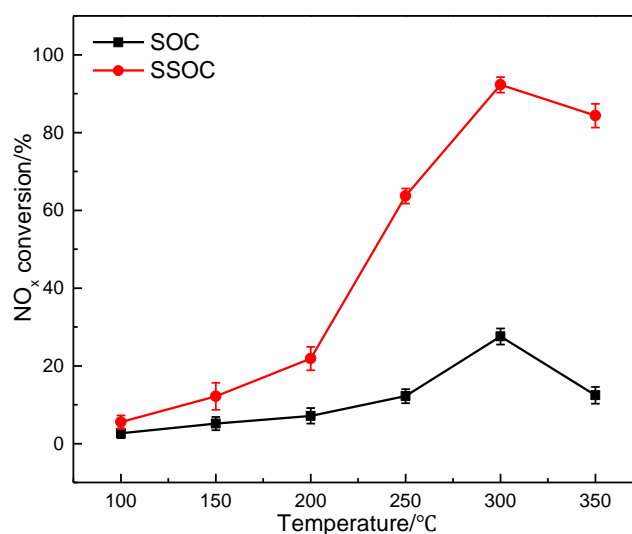


Figure 9. Effect of temperature on SCR activity on SOC and SSOC. 300 ppm NO, 15% O₂, Ar as balance gas, NH₃/NO ratio: 1.0, GHSV: 5000 h⁻¹.

The stability test of SSOC was shown at Figure 10. The reaction continued for 24 h at 300 °C, 1.0 NH₃/NO ratio, GHSV = 5000 h⁻¹. It could be seen that the NO_x conversion was stable at about 92%, which indicated that SSOC has a good denitration stability. Compared with the SOC, the denitration performance had been greatly improved after the acidification with sulfuric acid. The adsorption of NH₃ and NO on SSOC was obviously improved, which subsequently promoted the NH₃-SCR reaction.

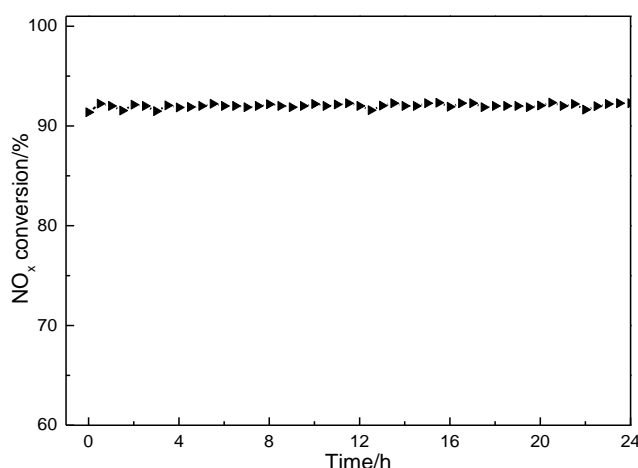


Figure 10. The stability test of SSOC. 300 ppm NO, 15% O₂, Ar as balance gas, NH₃/NO ratio: 1.0, GHSV: 5000 h⁻¹.

3. Experimental Process

3.1. Catalyst Preparation

In this experiment, the sintered ore was sampled from a sintering workshop in Wuhan. The sintered ore was dried, milled and sieved to 0.15–0.25 mm, which was denoted as SOC. The SSOC was prepared by using an impregnation method. Firstly, 100 g sintered ore (0.15–0.25 mm) was weighed and put into a beaker, then 50 mL sulfuric acid solution with a concentration of 5 mol/L was added and stirred simultaneously for 30 min. After filtration and washing with the deionized water, the mixture was dried at 105 °C and then calcined at 500 °C for 3 h in the air atmosphere. Finally, the prepared SSOC were naturally cooled to the room temperature, then crushed and sieved to 0.15–0.25 mm.

3.2. Catalyst Characterization

The main chemical composition of the SOC and SSOC were analyzed by X-ray fluorescence spectroscopy (XRF) (ARL SMS-XY, Thermo Fisher Scientific Corp., Waltham, MA, USA). The specific surface area, pore volume and pore size distribution of the catalysts were measured by an automated adsorption analyzer (Micromeritics ASAP 2020, Micromeritics Corp., Norcross, GA, USA). The catalysts samples were firstly degassed at 240 °C for 4 h before the test, and the adsorption medium was liquid nitrogen. The nitrogen adsorption and desorption were analyzed at −196 °C using BET analyzer (Micromeritics ASAP 2020, Micromeritics Corp., Norcross, GA, USA). The surface area was calculated by using the BET method according to nitrogen adsorption data in the relative pressure (P/P_0) range of 0.01–1. X-ray diffraction (XRD; Rigaku RINT2000, Tokyo, Japan) was performed using CuK α radiation ($\lambda = 1.54056 \text{ \AA}$) to detect the crystalline phases of the samples. The analysis of XRD was referred to International Centre for Diffraction Data (ICDD). X-ray photoelectron spectroscopy (XPS, AXIS Ultra DLD, Shimadzu Corp., Kyoto, Japan) was used to determine the valence states of the surface atoms of the catalysts with Al K α radiation.

In-situ DRIFTS experiments were carried out in a FTIR spectrometer (FT-IR, Bruker Tensor II, Bruker optics Corp., Karlsruhe, Germany) equipped with an in-situ cell and a mercury-cadmium-telluride detector [34–37]. For the adsorption of NH₃ (or NO + O₂), the catalyst was exposed to a 20 mL/min NH₃ (or NO + O₂), which resulted in the variation with adsorption time of the DRIFT spectra, and argon purging was subsequently performed. In the reaction mechanism studies, the catalyst was pretreated in a flow of 20 mL/min NH₃ for 40 min, then was shifted NO + O₂ at 300 °C to get the DRIFT spectra. All spectra were recorded by accumulating 100 scans at a spectra resolution of 4 cm⁻¹.

4. Conclusions

In this paper, SSOC displayed an excellent catalytic denitration activity. There were some sulfates that appeared in SSOC after acidification with sulfuric acid solution, which provided more Brønsted acid sites. In-situ DRIFTS results demonstrated that there were Lewis and Brønsted acid sites simultaneously on the surfaces of SOC and SSOC. The acidification contributed to the increase of the Brønsted acid sites at SSOC, which improved the adsorption capacity of NH_3 and NO. NH_3 and NO were adsorbed on the surface of catalysts to form amide species ($-\text{NH}_2$), NH_4^+ species, NO_2 molecules in gaseous or weakly adsorbed state and nitrate species. Meanwhile, it could be seen that the NH_3 -SCR process of SOC and SSOC followed E-R and L-H mechanisms. Moreover, the optimum reaction temperature of catalysts was $300\text{ }^\circ\text{C}$ and maximum NO_x conversion fraction over SSOC was 92% at 1.0 NH_3/NO ratio and 5000 h^{-1} GHSV. It was observed that the NO_x conversion could be steadily maintained.

Author Contributions: Data curation, F.H.; Investigation, Y.T.; Methodology, L.Q.; Project administration, J.H.; Software, B.Z.; Writing—original draft, W.C.; Writing—review & editing, F.Y.

Funding: The present work was partly supported by the National Natural Science Foundation of China (Grant No. 51476118 and 51576146).

Conflicts of Interest: The authors declare no conflict of interest. The funders had no role in the design of the study; in the collection, analyses, or interpretation of data; in the writing of the manuscript, or in the decision to publish the results.

References

1. Zhou, H.; Chen, J.; Zhou, M.; Cen, K. Experimental investigation on the mixing performance of heating gas into the low temperature sintering flue gas selective catalyst reaction facilities. *Appl. Therm. Eng.* **2017**, *115*, 378–392. [[CrossRef](#)]
2. Ren, S.; Guo, F.; Yang, J.; Yao, L.; Zhao, Q.; Kong, M. Selection of carbon materials and modification methods in low-temperature sintering flue gas denitrification. *Chem. Eng. Res. Des.* **2017**, *126*, 278–285. [[CrossRef](#)]
3. Mousavi, S.; Panahi, P. Modeling and optimization of NH_3 -SCR performance of MnO_x/γ -alumina nanocatalysts by response surface methodology. *J. Taiwan Inst. Chem. Eng.* **2016**, *69*, 68–77. [[CrossRef](#)]
4. Han, J.; Liang, Y.; Hu, J.; Qin, L.; Street, J.; Lu, Y.; Yu, F. Modeling downdraft biomass gasification process by restricting chemical reaction equilibrium with Aspen Plus. *Energy Convers. Manag.* **2017**, *153*, 641–648. [[CrossRef](#)]
5. Ogidiana, O.; Shamim, T. Performance Analysis of Industrial Selective Catalytic Reduction (SCR) Systems. *Energy Procedia* **2014**, *61*, 2154–2157. [[CrossRef](#)]
6. Chen, C.; Cao, Y.; Liu, S.; Chen, J.; Jia, W. Review on the latest developments in modified vanadium-titanium-based SCR catalysts. *Chin. J. Catal.* **2018**, *39*, 1347–1365. [[CrossRef](#)]
7. Liu, F.; Asakura, K.; He, H.; Shan, W.; Shi, X.; Zhang, C. Influence of sulfation on iron titanate catalyst for the selective catalytic reduction of NO_x , with NH_3 . *Appl. Catal. B Environ.* **2011**, *103*, 369–377. [[CrossRef](#)]
8. Zhang, Q.; Fan, J.; Ning, P.; Song, Z.; Liu, X.; Wang, L.; Wang, J.; Wang, H.; Long, K. In situ DRIFTS investigation of NH_3 -SCR reaction over $\text{CeO}_2/\text{zirconium phosphate}$ catalyst. *Appl. Surf. Sci.* **2018**, *435*, 1037–1045. [[CrossRef](#)]
9. Chen, W.; Luo, J.; Qin, L.; Han, J. Selective autocatalytic reduction of NO from sintering flue gas by the hot sintered ore in the presence of NH_3 . *J. Environ. Manag.* **2015**, *164*, 146–150. [[CrossRef](#)]
10. Zhang, C.; Chen, T.; Liu, H.; Chen, D.; Xu, B.; Qing, C. Low temperature SCR reaction over Nano-Structured Fe-Mn Oxides: Characterization, performance, and kinetic study. *Appl. Surf. Sci.* **2018**, *457*, 1116–1125. [[CrossRef](#)]
11. Wang, X.; Gui, K. Fe_2O_3 particles as superior catalysts for low temperature selective catalytic reduction of NO with NH_3 . *J. Environ. Sci.* **2013**, *25*, 2469–2475. [[CrossRef](#)]
12. Yang, S.; Liu, C.; Chang, H.; Ma, L.; Qu, Z.; Yan, N.; Wang, C.; Li, J. Improvement of the activity of $\gamma\text{-Fe}_2\text{O}_3$ for the selective catalytic reduction of NO with NH_3 at high temperatures: No reduction versus NH_3 oxidization. *Ind. Eng. Chem. Res.* **2013**, *52*, 5601–5610. [[CrossRef](#)]
13. Shi, X.; He, H.; Xie, L. The effect of Fe species distribution and acidity of Fe-ZSM-5 on the hydrothermal stability and SO_2 and hydrocarbons durability in NH_3 -SCR reaction. *Chin. J. Catal.* **2015**, *36*, 649–656. [[CrossRef](#)]
14. Han, J.; He, X.; Qin, L.; Chen, W.; Yu, F. NO_x removal coupled with energy recovery in sintering plant. *Ironmak. Steelmak.* **2013**, *41*, 350–354. [[CrossRef](#)]

15. Chen, W.; Li, Z.; Hu, F.; Qin, L.; Han, J.; Wu, G. In-situ DRIFTS investigation on the selective catalytic reduction of NO with NH₃ over the sintered ore catalyst. *Appl. Surf. Sci.* **2018**, *439*, 75–81. [[CrossRef](#)]
16. Ciambelli, P.; Fortuna, M.; Sannino, D.; Baldacci, A. The influence of sulphate on the catalytic properties of V₂O₅-TiO₂ and WO₃-TiO₂ in the reduction of nitric oxide with ammonia. *Catal. Today* **1996**, *29*, 161–164. [[CrossRef](#)]
17. Khodayari, R.; Odenbrand, C. Regeneration of commercial SCR catalysts by washing and sulphation: Effect of sulphate groups on the activity. *Appl. Catal. B Environ.* **2001**, *33*, 277–291. [[CrossRef](#)]
18. Xu, T.; Wu, X.; Liu, X.; Cao, L.; Lin, Q.; Weng, D. Effect of barium sulfate modification on the SO₂ tolerance of V₂O₅/TiO₂ catalyst for NH₃-SCR reaction. *J. Environ. Sci.* **2017**, *57*, 110–117. [[CrossRef](#)] [[PubMed](#)]
19. Zhang, H.; Zou, Y.; Peng, Y. Influence of sulfation on CeO₂-ZrO₂ catalysts for NO reduction with NH₃. *Chin. J. Catal.* **2017**, *38*, 160–167. [[CrossRef](#)]
20. Liu, F.; He, H.; Ding, Y.; Zhang, C. Effect of manganese substitution on the structure and activity of iron titanate catalyst for the selective catalytic reduction of NO with NH₃. *Appl. Catal. B Environ.* **2009**, *93*, 194–204. [[CrossRef](#)]
21. Ma, L.; Seo, C.; Nahata, M.; Chen, X.; Li, J.; Schwank, J. Shape dependence and sulfate promotion of CeO₂ for selective catalytic reduction of NO_x with NH₃. *Appl. Catal. B Environ.* **2018**, *232*, 246–259. [[CrossRef](#)]
22. Liu, J.; Guo, R.; Li, M.; Sun, P.; Liu, S.; Pan, W. Enhancement of the SO₂ resistance of Mn/TiO₂ SCR catalyst by Eu modification: A mechanism study. *Fuel* **2018**, *223*, 385–393. [[CrossRef](#)]
23. Ramis, G.; Larrubia, M. An FT-IR study of the adsorption and oxidation of N-containing compounds over Fe₂O₃/Al₂O₃ SCR catalysts. *J. Mol. Catal. A Chem.* **2004**, *215*, 161–167. [[CrossRef](#)]
24. Kumar, P.; Jeong, Y.; Gautam, S.; Ha, H.; Lee, K.; Chae, K. XANES and DRIFTS study of sulfated Sb/V/Ce/TiO₂ catalysts for NH₃-SCR. *Chem. Eng. J.* **2015**, *275*, 142–151. [[CrossRef](#)]
25. Yu, C.; Huang, B.; Dong, L.; Chen, F.; Liu, X. In situ FT-IR study of highly dispersed MnO_x/SAPO-34 catalyst for low-temperature selective catalytic reduction of NO_x by NH₃. *Catal. Today* **2017**, *281*, 610–620. [[CrossRef](#)]
26. Zhang, L.; Qu, H.; Du, T.; Ma, W.; Zhong, Q. H₂O and SO₂ tolerance, activity and reaction mechanism of sulfated Ni-Ce-La composite oxide nanocrystals in NH₃-SCR. *Chem. Eng. J.* **2016**, *296*, 122–131. [[CrossRef](#)]
27. Chen, L.; Niu, X.; Li, Z.; Dong, Y.; Zhang, Z.; Yuan, F.; Zhu, Y. Promoting catalytic performances of Ni-Mn spinel for NH₃-SCR by treatment with SO₂ and H₂O. *Catal. Commun.* **2016**, *85*, 48–51. [[CrossRef](#)]
28. Li, X.; Li, K.; Peng, Y.; Li, X.; Zhang, Y.; Wang, D.; Chen, J.; Li, J. Interaction of phosphorus with a FeTiO_x catalyst for selective catalytic reduction of NO_x with NH₃: Influence on surface acidity and SCR mechanism. *Chem. Eng. J.* **2018**, *347*, 173–183. [[CrossRef](#)]
29. Liu, N.; Wang, J.; Wang, F.; Liu, J. Promoting effect of tantalum and antimony additives on deNO_x performance of Ce₃Ta₃SbO_x for NH₃-SCR reaction and DRIFT studies. *J. Rare Earths* **2018**, *36*, 594–602. [[CrossRef](#)]
30. Cao, L.; Chen, L.; Wu, X.; Ran, R.; Xu, T.; Chen, Z.; Weng, D. TRA and DRIFTS studies of the fast SCR reaction over CeO₂/TiO₂ catalyst at low temperatures. *Appl. Catal. A Gen.* **2018**, *557*, 46–54. [[CrossRef](#)]
31. Pen, D.; Uphade, B.; Reddy, E.; Smirniotis, P. Identification of Surface Species on Titania-Supported Manganese, Chromium, and Copper Oxide Low-Temperature SCR Catalysts. *J. Phys. Chem. B* **2004**, *108*, 9927–9936. [[CrossRef](#)]
32. Han, J.; Zhang, L.; Zhao, B.; Qin, L.; Wang, Y.; Xing, F. The N-doped activated carbon derived from sugarcane bagasse for CO₂ adsorption. *Ind. Crop. Prod.* **2019**, *128*, 290–297. [[CrossRef](#)]
33. Wang, H.; Qu, Z.; Dong, S.; Tang, C. Mechanism study of FeW mixed oxides to the selective catalytic reduction of NO_x with NH₃: In situ DRIFTS and MS. *Catal. Today* **2018**, *307*, 35–40. [[CrossRef](#)]
34. Han, J.; Li, W.; Liu, D.; Qin, L.; Chen, W.; Xing, F. Pyrolysis characteristic and mechanism of waste tyre: A thermogravimetry-mass spectrometry analysis. *J. Anal. Appl. Pyrolysis* **2018**, *129*, 1–5. [[CrossRef](#)]
35. Han, J.; Zhang, L.; Lu, Y.; Hu, J.; Cao, B.; Yu, F. The effect of syngas composition on the Fischer Tropsch synthesis over three-dimensionally ordered macro-porous iron based catalyst. *Mol. Catal.* **2017**, *440*, 175–183. [[CrossRef](#)]
36. Lu, Y.; Yan, Q.; Han, J.; Cao, B.; Street, J.; Yu, F. Fischer-Tropsch synthesis of olefin-rich liquid hydrocarbons from biomass-derived syngas over carbon-encapsulated iron carbide/iron nanoparticles catalyst. *Fuel* **2017**, *193*, 369–384. [[CrossRef](#)]
37. Huang, Z.; Qin, L.; Xu, Z.; Chen, W.; Xing, F.; Han, J. The effects of Fe₂O₃ catalyst on the conversion of organic matter and bio-fuel production during pyrolysis of sewage sludge. *J. Energy Inst.* **2018**. [[CrossRef](#)]

